Journal Pre-proofs

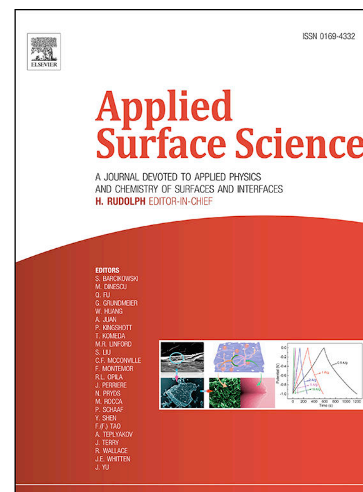

Full Length Article

AlN/diamond interface nanoengineering for reducing thermal boundary resistance by molecular dynamics simulations

Zijun Qi, Wei Shen, Rui Li, Xiang Sun, Lijie Li, Qijun Wang, Kang Liang, Gai Wu

PII:	S0169-4332(23)00095-8
DOI:	https://doi.org/10.1016/j.apsusc.2023.156419
Reference:	APSUSC 156419

To appear in: *Applied Surface Science*

Received Date:	26 November 2022
Revised Date:	1 January 2023
Accepted Date:	10 January 2023

Please cite this article as: Z. Qi, W. Shen, R. Li, X. Sun, L. Li, Q. Wang, K. Liang, G. Wu, AlN/diamond interface nanoengineering for reducing thermal boundary resistance by molecular dynamics simulations, *Applied Surface Science* (2023), doi: https://doi.org/10.1016/j.apsusc.2023.156419

This is a PDF file of an article that has undergone enhancements after acceptance, such as the addition of a cover page and metadata, and formatting for readability, but it is not yet the definitive version of record. This version will undergo additional copyediting, typesetting and review before it is published in its final form, but we are providing this version to give early visibility of the article. Please note that, during the production process, errors may be discovered which could affect the content, and all legal disclaimers that apply to the journal pertain.

© 2023 Published by Elsevier B.V.

AlN/diamond interface nanoengineering for reducing thermal boundary resistance by molecular dynamics simulations

Zijun Qi[1,†], Wei Shen[1,2,4,†], Rui Li[1], Xiang Sun[1,2], Lijie Li[3], Qijun Wang[1], Kang Liang[1,2,4,*], Gai Wu[1,2,4,*]

[1] The Institute of Technological Sciences, Wuhan University, Wuhan 430074, China

[2] School of Power and Mechanical Engineering, Wuhan University, Wuhan, 430072, China

[3] College of Engineering, Swansea University, Swansea, SA1 8EN, UK

[4] Research Institute of Wuhan University in Shenzhen, Shenzhen, 518057, China

[*] Corresponding authors:

wugai1988@whu.edu.cn (Gai Wu)

liangkang@whu.edu.cn (Kang Liang)

[†] Zijun Qi and Wei Shen contributed equally to this work.

Journal Pre-proofs

Abstract

Interfacial thermal transport has become a significant bottleneck in thermal management, particularly for the electronic high-power devices represented by Ⅲ-Ⅴ semiconductor devices. Diamond has great potential to be integrated with devices to dissipate heat efficiently due to its ultra-high thermal conductivity. In this paper, the Non-equilibrium Molecular Dynamics method, taking into consideration of the parameters such as the type of the interleaved nanopillars, the size and the height of the nanopillars, was used to study the influence of nanopillars on the thermal boundary

resistance (TBR) at AlN/diamond interfaces. The TBR of the optimal AlN/diamond interface of nanopillar structures could be reduced by 28% compared to the planar interface. The vibrational density of states (VDOS) analysis of both AlN and diamond on each side of the interface can reveal that the enhancement of AlN intermediate frequency phonons and the shift of diamond VDOS towards the lower frequency can contribute to the optimization of the interfacial thermal transport. Hence, this work can provide a deeper understanding of the impact of nanostructures on the interfacial thermal transport and can also be a guideline for efficient thermal management through the introduction of nanostructures at the heterogeneous interfaces.

Keywords: Thermal boundary resistance; AlN/diamond interface; Nanostructure; Molecular dynamics

1 Introduction

Advances in power electronics and materials technology have contributed to a sharp increase in the power density of semiconductor devices. The accompanying excessive heat flux leads to a significant increase in the junction temperature of high-power electronic devices, which degrades the electron transport performance and seriously threatens the reliability of the devices. Due to the outstanding properties such as high breakdown voltages, high electron mobility, and high switching speed, III-V semiconductors have been widely used to fabricate high-power and high-frequency devices in the applications of radio-frequency communications, medical technologies, industrial manufacturing, etc. However, the problem of heat dissipation is still a great challenge for the III-V semiconductors. For example, it is recently reported that the local power density of the high electron mobility transistors (HEMTs) based on Ⅲ-Ⅴ semiconductors could be as high as approximately 100 $kW \cdot cm^{-2}$, and the performance of the devices may be seriously limited due to the high operating temperature of the channel (~200℃) [1-3]. Therefore, efficient cooling of high-power devices is an urgent barrier that needs to be overcome.

Attaching electrically active device layers to highly thermally conductive materials is an effective way to optimize the thermal management. For example, GaN is a typical Ⅲ-Ⅴ semiconductor material with high breakdown electric field and high electron mobility, which is widely used in the fabrication of HEMTs. However, the low thermal conductivity of GaN material usually leads to local self-heating which will severely degrade the performance and reliability of the GaN devices [4, 5]. To achieve a more effective thermal management, the integration of diamond films and GaN HEMTs (GaN-on-diamond) has been proposed because of the excellent thermal conductivity of diamond (over 1000 $W \cdot m^{-1} \cdot K^{-1}$), which can rapidly extract heat from the junction [6, 7]. However, it is extremely challenging to achieve the GaN-on-diamond structure through direct bonding or heteroepitaxial growth because of the mismatch of lattice constants as well as the thermal expansion coefficient difference between GaN and diamond [8]. Therefore, a barrier layer is usually introduced to improve the crystalline quality of heteroepitaxial GaN film as well as reduce the thermal stress. However, due to the introduction of barrier layer, new interfaces will be generated and the phonon-dominated thermal boundary resistance (TBR) will become an important obstacle to the thermal transport in electronic power devices [9]. The TBR characterization could be performed by the optical methods (e.g. the transient thermal reflection method) and electrical methods (e.g. the 3ω method), and Cao, et al. have proposed a two-sensor 3ω-2ω method, which could overcome the shortcomings of the conventional 3ω method to improve the accuracy of the measurement while maintaining the convenience of operation of the electrical method [10].

The substrate selected as a barrier layer can affect the overall thermal transport throughout the system due to its different thermal conductivity, thermal expansion coefficient and the surface roughness. The material and the surface structure of the substrate will have an important impact on the TBR. Optimizing barrier layer materials and adding nanostructures to the interface are two effective methods for reducing TBR [11, 12]. The first method can improve the quality of the interface and the matching of the phonon transmission. For example, SiN is currently a commonly used barrier

material for GaN-on-diamond, providing an excellent environment for seeding and growth of diamond on GaN. The smooth diamond/SiN and SiN/GaN interfaces can reduce the TBR caused by roughness and poor contact, but the inherently low thermal conductivity of SiN will hinder the heat dissipation of the active region. According to recent studies, the AlN material can be a promising candidate to replace silicon nitride [13, 14]. The lower limit of TBR for the AlN/diamond interface predicted by the diffuse mismatch model (DMM) theory is 0.8 $m^2 \cdot K \cdot GW^{-1}$, while the lowest value achieved is currently 16 $m^2 \cdot K \cdot GW^{-1}$ [15, 16]. Furthermore, fabricating nanostructures at the interface is a potential method to reduce the TBR. From a macro perspective, a more efficient cooling could be achieved by increasing the surface area. The fin-like nanostructures at the micro-nano scale have also been shown to be an effective method for optimizing interfacial thermal transport [12]. Chen et al. found that the thermal boundary conductance of Si/diamond interface with nanoscale trenches increased by 65% compared with that of a flat Si/diamond interface [17]. Experimental study by Lee, et al. showed that there existed an optimal interfacial contact area at the Al/Si nanostructured interface that could maximize the thermal conductivity [18]. Additionally, numerous theoretical studies on interfacial structure have been carried out, demonstrating the enhanced impact of nanostructures on interfacial thermal transport. Hua, et al. studied the thermal transport across nanostructured interfaces using a phonon Monte Carlo technique, and found that the improvements in thermal transport could be attributed to a combination of changes in the heat conduction pathway and the enhanced phonon transport, which could explain the variation of the effective thermal resistance ratio with the contacting area [19]. Liang and Sun's Non-equilibrium Molecular Dynamics (NEMD) study on double-layered thin films found that the staggered interface had a significant effect on thermal conductivity [20]. NEMD simulations by Hu, et al. and Tao, et al. demonstrated that nanostructures at GaN/AlN/SiC interface and GaN/diamond interface could improve the distribution and matching of the vibrational density of states (VDOS), which could enhance the phonon transport at interface and achieve a more efficient thermal transport [21, 22]. For achieving the more

Journal Pre-proofs

accurate thermal transport simulations, A. M. Joseph, et al. proposed a new Monte Carlo method for simulating thermal transport in materials, which considered the electron-phonon interaction (EPI). The results showed that the EPI had a significant impact on the room temperature thermal conductivity of the material [23]. M. Khalkhali, et al. studied the relationship between molecular dynamics temperature and quantum temperature and obtained more accurate simulations of heat transport in silicon nanowires through quantum correction， which had an important significance for the molecular dynamics calculations below Debye temperature [24].

In this work, 56 interface models have been established by introducing the nanostructures into the AlN/diamond interface. The TBRs of these models, which are characterized by the type, size and height of the nanopillars, have been studied by NEMD. Multiple sets of parameters which enable TBR optimization are obtained and the mechanism behind the optimization of interfacial thermal transport via nanostructures is investigated by analyzing the vibrational density of states. It is the enhancement of the intermediate frequency of AlN phonons and the movement of diamond VDOS to the low-frequency that contribute to the improvement of interfacial thermal transport. As there are few previous studies reporting on the atomistic simulations of the thermal transport of the AlN/diamond system as well as the effect of nanostructures at the AlN/diamond interface on the thermal transport, this research is believed to provide a powerful guidance for the achievement of more efficient thermal management and the fabrication of power devices of higher power handling capability and reliability.

2 Method

2.1. Model structures

In the case studied in NEMD, each model consists of a heterostructure formed by diamond and AlN. Diamond and AlN have diamond cubic lattice structure and wurtzite

Journal Pre-proofs

crystal structure, respectively, with lattice constants of $a_{diamond}$ = 3.567 Å and a_{AlN} = 3.112 Å. As the (0001) surface is the most commonly-used surface for the fabrication of AlN-based HEMT, MEMS and other devices due to the spontaneous polarization and piezoelectric polarization properties of the group-III nitrides in the c-axis direction, the (0001) crystallographic plane is selected as the surface of the AlN layer [25]. Thus, the plane (0001) was set as the *x*-*y* plane, and the c-axis of diamond and AlN extends in the *z*-direction (thermal transport direction). Under this layout, considering the different lattice constants of diamond and AlN, the base model of AlN/diamond heterostructure with a planar interface is designed with the dimensions of 124.85 Å × 124.85 Å × 200.95 Å, where the mismatch between AlN and diamond in the *xy* plane is 1%. To study the effect of nanostructures on interfacial thermal transport, three series of interface configurations have been designed: the interface with diamond nanopillars embedded in AlN, the interface with AlN nanopillars embedded in the diamond, and the interlaced interface with both diamond nanopillars and AlN nanopillars. In this paper, the first two interfaces that contain only one type of nanopillars are called the unidirectional nanopillar interfaces and the third interface made up of two types of nanopillars is defined as the bidirectional nanopillar interfaces. The size of the nanopillars ranges from 10 to 60 Å, and the height of the nanopillars varies from 10 to 40 Å. In this work, a total of 56 MD models are built for NEMD simulations and the calculation of VDOS.

2.2. Molecular dynamics simulation

All the molecular dynamics (MD) simulations have been performed with the LAMMPS package [26]. Periodic boundary condition was applied in *x* and *y* directions during the simulation. To ensure the total energy stability of the complex systems, 0.5 fs was chosen as the time steps. The Tersoff three-body potential was employed to describe the atomic interactions in the AlN/diamond systems. The parameters for Al-N, N-N, and Al-Al interactions were obtained from the previous work of Tungare, et

Journal Pre-proofs

al. and Nord, et al. [27, 28]. For C-C interactions, the parameters were based on the previous work of Erhart, et al. [29]. By mixing the single-element Tersoff parameters, the C-Al and C-N interatomic interactions could be described by the analytical bond-order potential (ABOP) method, which was successfully used in the simulation of thermal transport in numerous previous literatures [21, 22, 30].

Table 1

Tersoff parameters for Al, N and C.

	C [29]	Al [27]	N [28]	Al-N [27]
D0 (eV)	6.00	1.5000	9.9100	3.3917
r_0 (Å)	1.4276	2.4660	1.1100	1.8616
S	2.167	2.7876	1.4922	1.7269
β (Å^{-1})	2.0099	1.0949	2.0595	1.7289
γ	0.11233	0.3168	0.7661	0.0000011
c	181.910	0.0748	0.1785	100390
d	6.28433	19.5691	0.2017	16.2170
h	0.5556	-0.6593	0.0452	-0.5980
2μ (Å^{-1})	0.0	1.5000	0.0	0.0
R (Å)	2.00	2.7000	2.2000	2.3400
D (Å)	0.15	0.1000	0.2000	0.1500

Four stages have been involved in the NEMD simulation. First, the system energy was minimized by using the conjugate gradient (CG) algorithm. In the second stage, the system was relaxed at constant temperature (300 K) and pressure (1 atm) for 0.15 ns using NPT (constant particles, pressure, and temperature) ensemble. After the NPT relaxation, the system was relaxed for 0.1 ns under the NVE (constant volume and no thermostat) ensemble. At the end of the NVE relaxation phase, the system energy converged well and the temperature stayed around 300 K with very small fluctuations.

Journal Pre-proofs

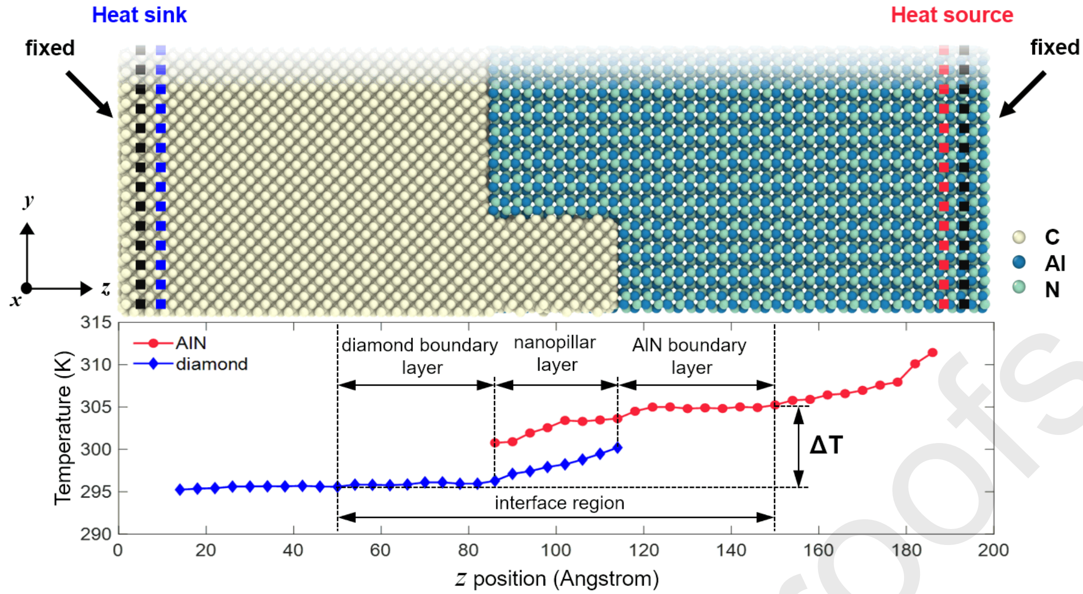

Fig. 1. (Upper) Typical nanostructured heterojunction of AlN/diamond. The yellow, blue and green atoms represent C, Al and N, respectively. (Lower) The corresponding temperature profiles. Red dotted curve and blue prismatic curve represent the temperature profiles of AlN and diamond, respectively. The interface region is defined as the range between 50 Å and 150 Å on the *z*-axis and then is further divided into the nanopillar layer, diamond boundary layer and AlN boundary layer according to the length of the nanopillar.

Fig. 1 shows a typical model of the nanostructured heterostructure. The TBR of the AlN-Diamond junction was obtained by using nonequilibrium molecular dynamics modeling in the last step. The atoms at both ends of the model along the *z* direction (perpendicular to the AlN/diamond interface) were fixed to form adiabatic walls while the remaining atoms were still in the NVE ensemble. The heat source and heat sink were then positioned in diamond and AlN, respectively, close to the adiabatic walls. The Jund–Julien algorithm was used to exchange energy between the heat source and the heat sink with a fixed heat flux [31]. The model was divided into 50 slices along the *z* direction, and the temperature of each slice was calculated from the kinetic energy to obtain the temperature profile. Each slice had a thickness of approximately 4 Å and contained about 7000-14000 atoms, which ensured a minimal variation in temperature fluctuations. After testing, a heat flux of 500 $kW \cdot cm^{-2}$ for 0.3 ns was chosen to be applied to all the models for calculating a stable temperature profile, and the results

were averaged over 0.1 ns for reducing the random error of calculation. The heat flux J_Q could be calculated as:

$$J_Q = \frac{\frac{dQ}{dt}}{A} \#(1.)$$

where dQ/dt is the thermal energy across the cross section of the model per unit time, and A is the cross-sectional area of the model. In order to reduce the influence of the interface area division, the interface region of the model was set to a uniform size. The temperature difference ΔT was obtained from the temperature profiles of the interface region mentioned above. Referring to the Refs. [15], TBR could be defined as the analogy of thermal conductivity and calculated as:

$$TBR = \frac{\Delta T}{J_Q} \#(2.)$$

Additionally, in order to further study the internal distribution and variation trend of TBR at the interface, the interface region was further divided into the nanopillar layer, diamond boundary layer and AlN boundary layer, and the temperature differences of each layer were calculated.

3 Results and discussion

In this section, the thermal conductivities of AlN and diamond were calculated separately using the nonequilibrium molecular dynamics simulations (NEMD) and the size effects were observed when calculating the thermal conductivities of models with different lengths. The macroscopic thermal conductivities of AlN and diamond were further determined. Then the thermal transports of 56 interface models were simulated by NEMD and the TBR was calculated by the temperature profile. Finally, the mechanism underlying the influence of nanostructure on interfacial thermal transport was investigated by comparing the vibrational density of states (VDOS) of various AlN/diamond interfaces.

Journal Pre-proofs

3.1. Size effects

In order to confirm the applicability of the potential function, the NEMD has been used to calculate the thermal conductivity of diamond and AlN, respectively. Considering the superior thermal conductivity of diamond, the heat flux given to the diamond model was 1.7 times more than that of AlN to produce a temperature profile with a clear slope. Using the model with a length of 200 Å, the calculated results of thermal conductivity of diamond and AlN are 97 $W \cdot m^{-1} \cdot K^{-1}$ and 23 $W \cdot m^{-1} \cdot K^{-1}$, respectively. It can be found that the simulation results are clearly lower than the experimental data, and this is because the phonon mean free path (MFP) of diamond and AlN in the actual thermal conduction process are 100 nm and 2500 nm, respectively [32, 33]. The small size of the model affects the MFP in the simulation process, which leads to the lower calculated thermal conductivity. However, due to the limitation of the computing capability, it is not practical to build a model with size larger than the phonon mean free path for simulation, but the corresponding thermal conductivity in the case of $L \rightarrow \infty$ can be fit through the simulation of a series of models with the increasing length [34]. In the thermal transport simulations, the effect of the model length on the temperature distribution can be intuitively seen from Fig. 2.

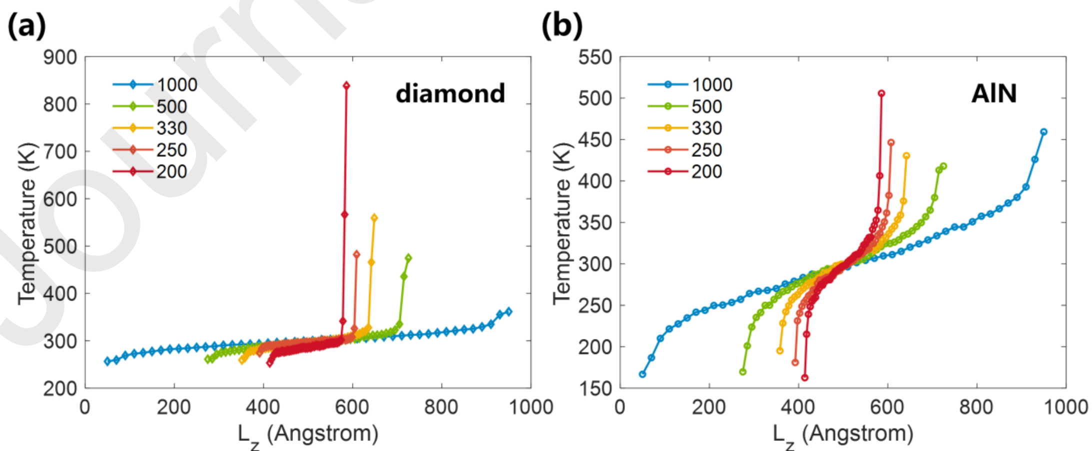

Fig. 2. Comparison of the temperature profile of (a) diamond and (b) AlN with different model lengths (200, 250, 330, 500, 1000 Å)

Fig. 2 (a) and (b) show the temperature gradient of AlN and diamond with different lengths. Apart from the drastic temperature changes in the heat source region and the heat sink region, the middle section of the curve shows the characteristic slope. As can be seen from the temperature distribution curves in the middle part of a series of models, the temperature gradient gradually decreases with the increase of model size, which indicates that the thermal conductivity displayed by the model gradually increases. The relationship between κ^{-1} and L_z^{-1} of Si under the influence of size effects in the simulation process is given in the literature [34]:

$$\frac{1}{\kappa}=\frac{a^3}{4k_B\upsilon}\left(\frac{1}{l_\infty}+\frac{4}{L_z}\right)\#(3.)$$

where κ is the thermal conductivity, a is the lattice constant, k_B is Boltzmann's constant, υ is the phonon group velocity of the material, l_∞ is the phonon mean free path, and L_z is the length of model in the direction of heat flow. A simplified linear relation between κ^{-1} and L_z^{-1} can be obtained by analogy:

$$\frac{1}{\kappa}=m\frac{1}{L_z}+n\#(4.)$$

where m and n are the characteristic coefficients that depend on the material. Fig. 3 shows the linear relationship between the thermal conductivity and the model length fit by the least square method. When $L_z^{-1}\rightarrow 0$ ($L_Z\rightarrow\infty$), the reciprocal of the intersection point between the fitting line and the 1/k axis is the deduced thermal conductivity at the macroscopic size. For each model of different lengths, we have repeated the simulation for five times and the results are shown in Fig. 3. The fitting results show the derived thermal conductivity of the macroscopic sizes of diamond and AlN are 1161 $W\cdot m^{-1}\cdot K^{-1}$ and 218 $W\cdot m^{-1}\cdot K^{-1}$, respectively, which are very close to the experimental results and indicate that the empirical potential has a good performance in heat transport simulation.

Journal Pre-proofs

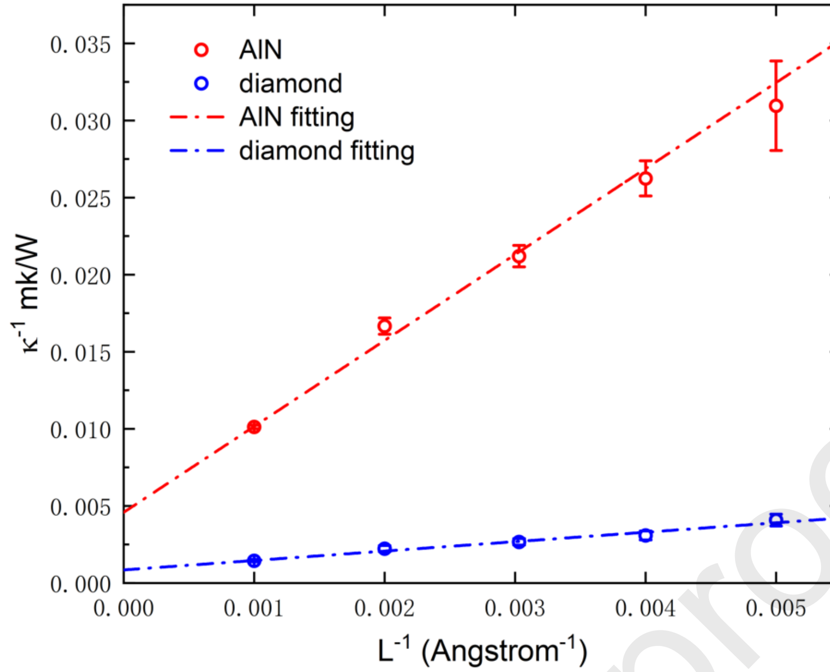

Fig. 3. Dependence of thermal conductivity (k^{-1}) on model size (L^{-1}). Red and blue circles represent the calculated thermal conductivity of AlN and diamond, respectively. Red and blue dashed lines are the least squares fit to the calculated data, and the intersection points with the vertical axis are 4.59×10^{-3} m·K·W^{-1} and 8.61×10^{-4} m·K·W^{-1}, respectively.

3.2. Non-equilibrium MD (NEMD) determination of the thermal boundary resistance

To reduce the thermal boundary resistance of the AlN/diamond interface and realize the optimal configuration of the interface structure, three series of interfacial structures have been built and extensive NEMD simulations have been conducted.

Journal Pre-proofs

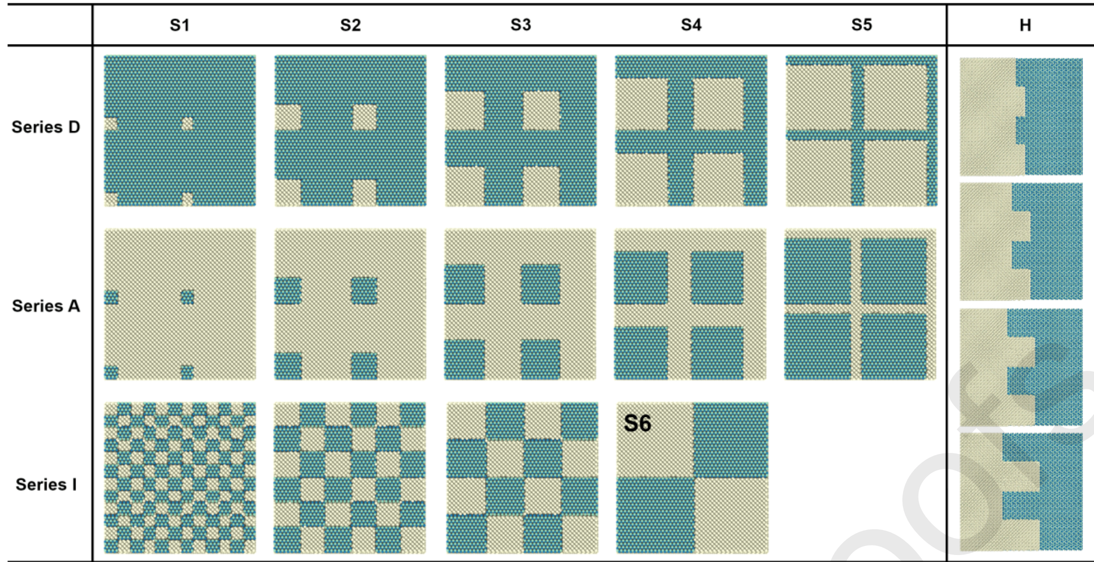

Fig. 4. Cross-sectional view of nanostructured AlN/diamond interfaces and side view of the nanopillars. All interface configurations are determined by three nanopillar characteristics: nanopillars type (Series D: diamond nanopillars; Series A: AlN nanopillars; Series I: interlaced interface with both diamond nanopillars and AlN nanopillars), size (S1-S6: from 1×1 to 6×6 nm^2) and height (H: from 1 to 4 nm).

As shown in Fig. 4, the factors that characterize the interfacial nanostructure include: the material of nanopillar at the interface (diamond, AlN, both diamond and AlN), the size of nanopillar (from 1×1 to 6×6 nm^2), and the height of nanopillar (from 1 to 4 nm). In general, the thermal transport of 56 cases in 3 series of the nanostructured interfaces have been performed and the TBR of each interface has been calculated. The label of each case could be described by the material, size, and height of the nanopillar at the interface. Taking the label "I-S2-H3" as an example, the first symbol "I" indicates the interlaced interface composed of both diamond nanopillars and AlN nanopillars, and other symbols "A" and "D" refer to the AlN nanopillar interface and diamond nanopillar interface, respectively. "S2-H3" refers to the nanopillar size of 2×2 nm^2 and height of 3 nm.

Journal Pre-proofs

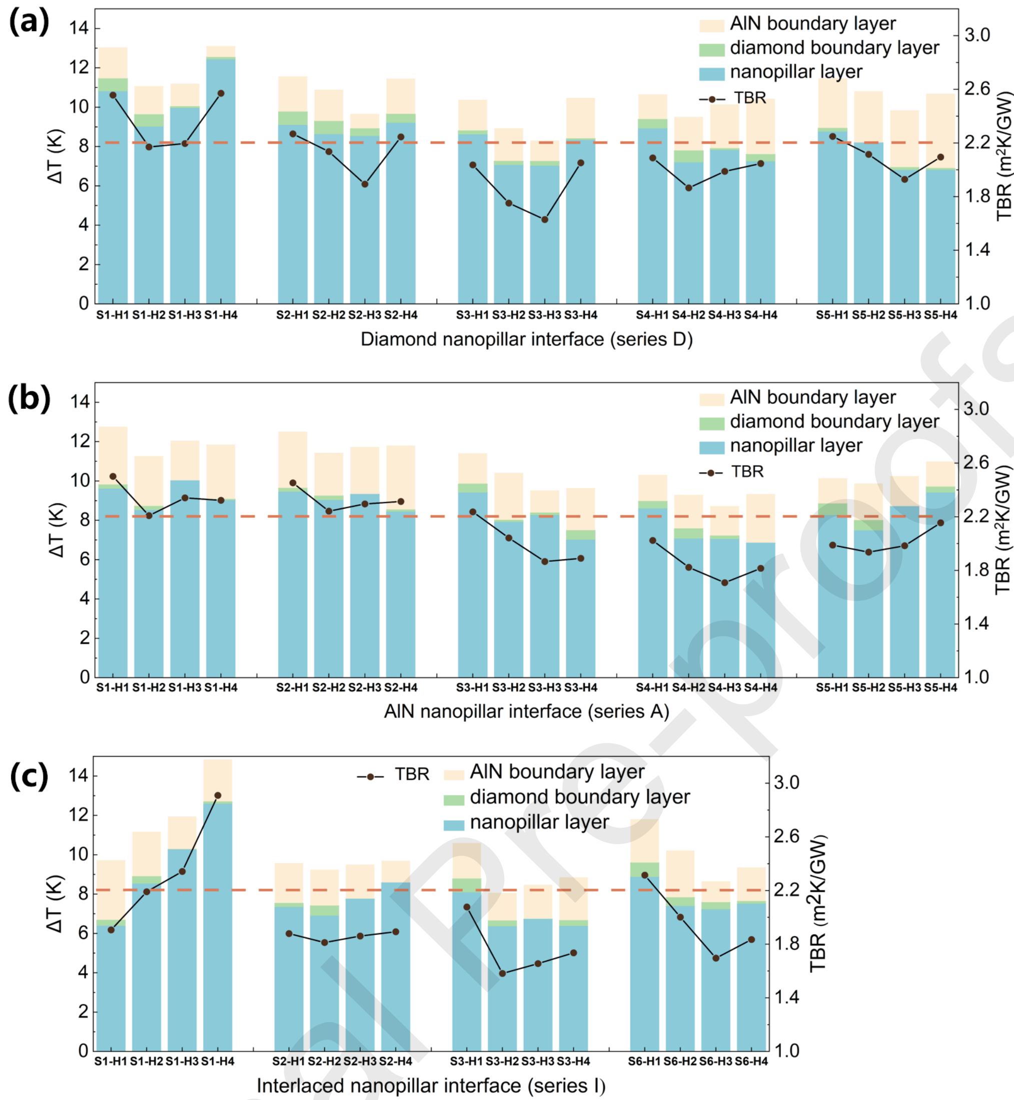

Fig. 5. TBR values (point and line diagram) and temperature difference contribution (histogram) of nanopillar layer, diamond boundary layer and AlN boundary layer: (a) Diamond nanopillar interface (series D); (b) AlN nanopillar interface (series A); (c) Interlaced interface (series I). The dashed line represents the TBR of the planar interface.

Journal Pre-proofs

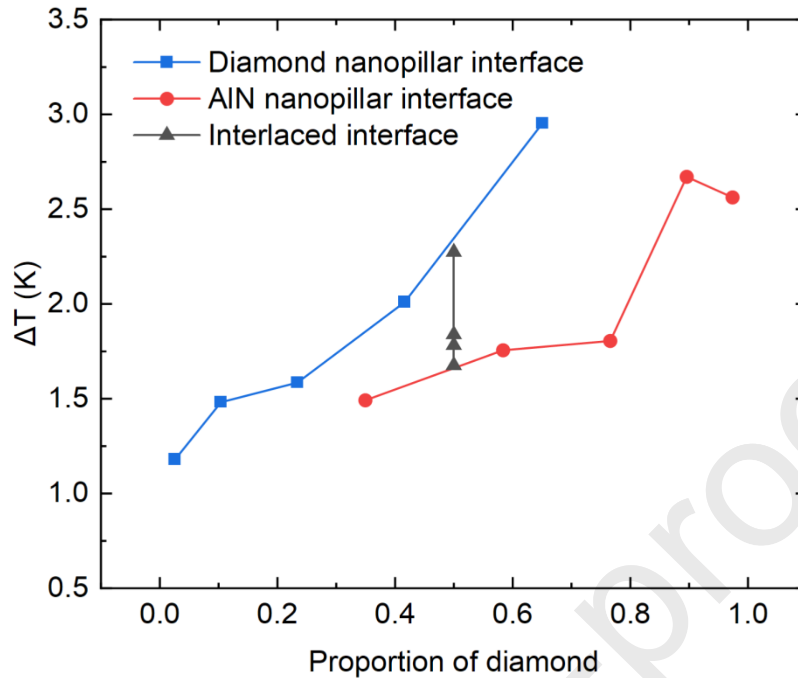

Fig. 6. The temperature difference (ΔT) of AlN boundary layer as a function of the diamond proportion. Each point represents the average of the temperature differences for interface with the same material and size of nanopillars but different height.

Fig. 5 shows the TBR values and contribution of temperature difference at the interface for 56 cases of simulations. The dashed line represents the TBR of the planar interface. First, in the configuration with the same nanopillar material and size, the TBR value generally decreases first and then increases with the increase of nanopillar height. It can be observed that in all groups with the nanopillar height as a variable, excluding the group I-S1-Hx, the minimum TBR in the group appears in the models when the nanopillar height is 2 or 3 nm. This can be attributed to the fact that the side walls of the nanopillars can increase the interfacial scattering of phonons to reduce the interfacial thermal resistance. However, when the size of the nanopillars is smaller than the phonon mean free path of the material, the overall backscattering of phonons increases subsequently (especially noticeable in I-S1-Hx) as the nanopillar height further increases [35]. The above two mechanisms could result in a U-shaped TBR curve and an optimal nanopillar height, as shown in Fig. 5. Second, all three series of

Journal Pre-proofs

the small size nanopillar are not effective in optimizing the thermal boundary resistance but even inhibiting the interfacial thermal transport. It can be observed that in the AlN nanopillar series, the lowest TBR in the group of nanopillar sizes of 1 × 1 and 2 × 2 nm^2 (A-S1-Hx and A-S2-Hx) is even larger than the TBR of the planar interface. Half of the TBRs in D-S1-Hx and D-S2-Hx are larger than that of the planar interface in the diamond nanopillar series. This is because small nanopillars can offer extremely thin sidewalls that enable phonon scattering, and therefore the small nanopillars cannot effectively enhance thermal transport at the interface. On the contrary, due to the lattice mismatch, this would be considered a defect impeding the thermal transport at the interface. In the series “I”, the TBR from I-S1-H1 to I-S1-H4 gradually increases and is finally significantly larger than that of the planar interface. Compared with the series “A” and “D”, the series “I” have a higher nanopillar density, which provides larger side walls for enhancing phonon transport despite the small size of nanopillar, and thus I-S1-H1 and I-S1-H2 show better interfacial heat transfer. However, the enhanced phonon backscattering from the increased nanopillar height mentioned above leads to an increase in TBR of I-S1-H4. Additionally, as shown in Fig. 6, in the series “A” and “D”, the temperature difference of the AlN boundary layer increases as the proportion of diamond in the cross-section of the nanopillar layer increases. The composition of the total thermal resistance can be divided into the thermal resistance of the nanopillar layer, the diamond boundary layer and the AlN boundary layer. Since the thicknesses of these three layers are varying with the nanopillars, which introduces the inconsistent variables, it is not appropriate to compare the values calculated by the $\Delta T/J_Q$ mode. Thus, temperature difference is used to reflect the thermal resistance of each layer's contribution to the whole TBR of the interface. From Fig. 5, it can be seen that the thermal resistance of the nanopillar layer accounts for 78% - 98% of the total thermal resistance, while the thermal resistance of the diamond boundary layer is only a small and negligible fraction, and the remaining AlN boundary layer thermal resistance exhibits a correlation with the proportion of diamond in the cross-section of the nanopillar layer, which is especially obvious in the series “A”. The average thermal

Journal Pre-proofs

resistance of the AlN side increases as the percentage of diamond in the cross-section increases. Eventually, among the 56 interfacial nanostructures, the interfacial nanostructure having an interlaced interface with the nanopillar size of 3×3 nm^2 and height of 2 nm (I-S3-H2) has the lowest TBR of 1.58 m^2·K·GW^{-1}, which results in a 28% decrease in TBR compared to the planar interface (2.2 m^2·K·GW^{-1}). The lowest TBR obtained in series "A" and "D" are 1.71 m^2·K·GW^{-1} and 1.62 m^2·K·GW^{-1}, respectively, which achieve optimization effect without too many changes in the interface compared with the interlaced interface.

3.3. Vibrational density of states of the interface

Analyzing the atomic vibrational density of states is a useful method to comprehend the impact of nanostructures on thermal boundary resistance since the vibrational characteristics of atoms at the near interface play a significant role in phonon transport. In this part of the study, Fourier transformation of the atomic velocity autocorrelation function has been used to calculate the VDOS [36]:

$$D(\omega) = \int_0^\infty \left\langle \vec{v}(t)\vec{v}(0) \right\rangle e^{i\omega t} \mathrm{d}t \#(5.)$$

where $D(\omega)$ is the VDOS at frequency ω, and v is the atomic velocity. The MD simulations on thermal transport above demonstrate that some interfaces with nanostructures show superior interfacial thermal transport performance compared to flat interfaces, while some nanostructures impair interfacial thermal transport performance. In order to include the entire nanopillars at the interface, the relatively thick VDOS calculation blocks were set up, which contained a large number of atoms that were far away from the interface and not directly affected by the interface, which could reduce the contribution of vibrational variations of atoms at the interface to the whole VDOS. For comparison, the VDOS of the planar interface, the I-3-2 and D-3-2 interface (the configurations with the lowest TBR in series I and D, respectively) and the D-1-4 interface (with higher TBR than the planar interface) have been calculated. By comparing the details of VDOS of the planar interface and the nanopillar interfaces,

Journal Pre-proofs

the characteristic changes of atomic vibration at the interface could be inferred and the mechanisms behind the influence of interfacial nanostructures on TBR of the AlN/diamond interface could be analytically studied.

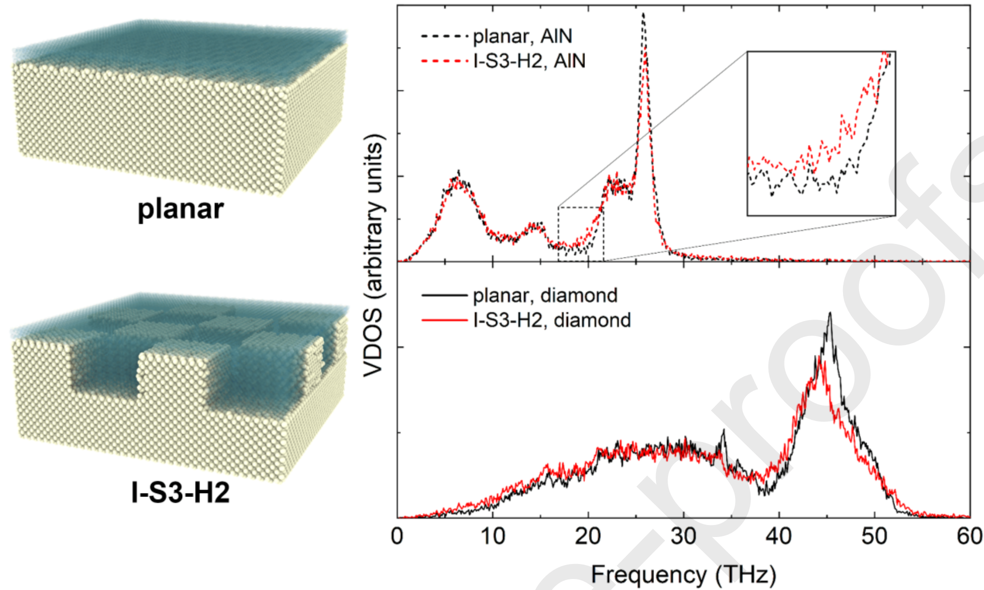

Fig. 7. Comparison of vibrational density of states (VDOS) of AlN and diamond between planar interface and interface I-S3-H2 (nanopillars of series I with size of 2 × 2 nm^2 and height of 3 nm).

Fig. 7 shows the VDOS of AlN and diamond at the planar interface and I-S3-H2. It can be observed that the VDOS of diamond$_{I\text{-}S3\text{-}H2}$ significantly moves toward the low frequency as compared with the planar interface. In general, the distribution of VDOS across different frequency ranges has an impact on thermal transport, and the low frequency (0-7 THz) phonons and the intermediate frequency (7-20 THz) phonons are dominant in thermal transport. Meanwhile, the VDOS of AlN is located at a lower frequency than that of diamond. Hence moving toward the low frequency improves both the phonon transport and the overlap of VDOS between AlN and diamond, which indicates the better vibration coupling and lower TBR at the interface. Moreover, the VDOS of AlN$_{I\text{-}S3\text{-}H2}$ shows an enhancement at 15-20 THz and the smoother peaks. The intermediate frequency phonons can greatly improve the thermal transfer because of its suitable transmission coefficient and phonon group velocity, and the smoother VDOS enables a richer phonon transfer frequency, which further strengthens the vibrational coupling with the diamond [37, 38].

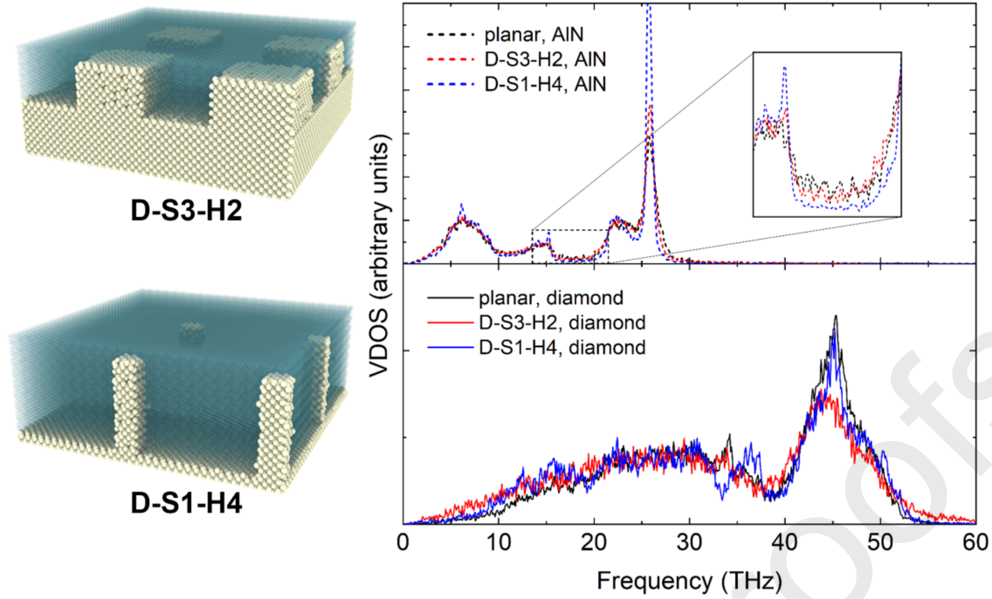

Fig. 8. Comparison of vibrational density of states (VDOS) of AlN and diamond between planar interface, interface D-S3-H2 (nanopillars of series D with size of 3 × 3 nm^2 and height of 2 nm) and D-S1-H4 (nanopillars of series I with size of 1 × 1 nm^2 and height of 4 nm).

The VDOS of D-S3-H2 and D-S1-H4 are illustrated in Fig. 8. It is clearly seen that the VDOS of $diamond_{D\text{-}S3\text{-}H2}$ shows a movement toward lower frequency, and a new peak appears at 15 THz which is in the same position as AlN in the VDOS of $diamond_{D\text{-}S1\text{-}H4}$. These new changes in the VDOS of diamond can improve the vibration coupling. There is basically no difference between the VDOS of AlN_{planar} and $AlN_{D\text{-}S3\text{-}H2}$, which can be attributed to the strong interaction between the contiguous bulk AlN. But the VDOS of $AlN_{D\text{-}S1\text{-}H4}$ at 15-20 THz is diminished and more phonons are distributed in high frequency with peaks becoming sharper. The sharp peaks restrict the transport channel of phonons and the high frequency (>20 THz) phonons contribute little to thermal transport due to the extremely low group velocities [22]. Considering the low percentage of diamond in D-S1-H4, the negative effects of nanostructures overwhelm optimization effects and eventually lead to a rise in TBR.

4 Conclusions

In summary, extensive simulations of the interfacial thermal conductance between AlN and diamond have been carried out. By using non-equilibrium MD and vibrational

Journal Pre-proofs

density of states calculations, the impact of three series of nanostructured interfaces on thermal boundary resistance and atomic vibration characteristics has been investigated. It is revealed from the simulation results of the 56 nanostructured interfaces that the interlaced interface can decrease the TBR by as much as 28% in comparison to the planar interface when the nanopillar size and height is 3×3 nm^2 and 2 nm, respectively (I-S3-H2). It can be found that the nanopillars of too small cross-section dimension is ineffective for reducing TBR. The increase of the diamond proportion in the nanopillar layer, which is determined by the nanopillar size, leads to an increase in the thermal resistance of the AlN boundary layer. Moreover, for the specific type of the interleaved nanopillars and size of the nanopillars, as the height of the nanopillar increases, the TBR always decreases at first and then increases, and thus a minimum value can be found. This is a result of the competition between phonon side walls scattering and backscattering. By analyzing the VDOS of AlN and diamond at the interface, two mechanisms behind optimizing TBR by nanostructured interfaces have been explained, which are the enhancement of the intermediate frequency of AlN phonons and the movement of diamond VDOS to the low-frequency. These changes to VDOS indicate the improvement of phonon coupling from both sides of the material at particular frequencies, which could reduce the TBR. Among the three types of interfaces, only the interlaced interface formed by the bidirectional nanopillars can optimize the atomic vibrations on both sides of the nanopillar interfaces, which could effectively enhance the mid-frequency phonons of AlN and shift the diamond VDOS to the low-frequency at the same time. The other two types of interfaces formed by the unidirectional nanopillars could provide optimization of atomic vibrations on only one side. Therefore, the bidirectional nanopillars have a wider window for the parameters of size and height to optimize the thermal transport of the interface and can achieve the lowest TBR, which makes the interlaced interface the optimal target among the three types of interfaces. This work can promote the understanding of the effect of nanostructures at heterostructure interface on thermal boundary resistance and can be a powerful

Journal Pre-proofs

guidance for design and fabrication of power devices of higher power and reliability in future.

Declaration of Competing Interest

The authors declare that they have no known competing financial interests or personal relationships that could have appeared to influence the work reported in this paper.

Acknowledgements

This work was supported by the National Natural Science Foundation of China (Grant No. 62004141, 52202045, 62204173), the Fundamental Research Funds for the Central Universities (Grant No. 2042022kf1028), the Guangdong Basic and Applied Basic Research Foundation (Grant No. 2020B1515120005, 2021A1515110890), and the Hubei Natural Science Foundation (Grant No. 2022CFB606).

References

[1] M.T. Barako, V. Gambin, J. Tice, Integrated nanomaterials for extreme thermal management: a perspective for aerospace applications, Nanotechnology, 29 (2018) 154003. https://doi.org/10.1088/1361-6528/aaabe1

[2] F. Ejeckam, D. Francis, F. Faili, D. Twitchen, B. Bolliger, D. Babic, J. Felbinger, S2-T1: GaN-on-diamond: A brief history, in: 2014 Lester Eastman Conference on High Performance Devices (LEC), IEEE, 2014. https://doi.org/10.1109/LEC.2014.6951556

[3] Y. Won, J. Cho, D. Agonafer, M. Asheghi, K.E. Goodson, Cooling Limits for GaN HEMT Technology, in: 2013 IEEE Compound Semiconductor Integrated Circuit Symposium (CSICS), IEEE, 2013. https://doi.org/10.1109/CSICS.2013.6659222

[4] M. Azarifar, N. Donmezer, A multiscale analytical correction technique for two-

Journal Pre-proofs

dimensional thermal models of AlGaN/GaN HEMTs, Microelectron. Reliab., 74 (2017) 82-87. https://doi.org/10.1016/j.microrel.2017.05.020

[5] R. Gaska, A. Osinsky, J.W. Yang, M.S. Shur, Self-heating in high-power AlGaN-GaN HFETs, IEEE Electron Device Lett., 19 (1998) 89-91. https://doi.org/10.1109/55.661174

[6] L. Yates, A. Sood, Z. Cheng, T. Bougher, K. Malcolm, J. Cho, M. Asheghi, K. Goodson, M. Goorsky, F. Faili, D.J. Twitchen, S. Graham, Characterization of the Thermal Conductivity of CVD Diamond for GaN-on-Diamond Devices, in: 2016 IEEE Compound Semiconductor Integrated Circuit Symposium (CSICS), IEEE, 2016. https://doi.org/10.1109/CSICS.2016.7751032

[7] Y. Won, J. Cho, D. Agonafer, M. Asheghi, K.E. Goodson, Fundamental Cooling Limits for High Power Density Gallium Nitride Electronics, Ieee Transactions on Components Packaging and Manufacturing Technology, 5 (2015) 737-744. https://doi.org/10.1109/Tcpmt.2015.2433132

[8] H. Amano, N. Sawaki, I. Akasaki, Y. Toyoda, Metalorganic vapor phase epitaxial growth of a high quality GaN film using an AlN buffer layer, Appl. Phys. Lett., 48 (1986) 353-355. https://doi.org/10.1063/1.96549

[9] M. Hu, D. Poulikakos, Graphene mediated thermal resistance reduction at strongly coupled interfaces, Int. J. Heat Mass Transfer, 62 (2013) 205-213. https://doi.org/10.1016/j.ijheatmasstransfer.2013.02.045

[10] Y.-C. Hua, B.-Y. Cao, A two-sensor 3 omega-2 omega method for thermal boundary resistance measurement, J. Appl. Phys., 129 (2021). https://doi.org/10.1063/5.0039444

[11] L. Zhang, G. Ouyang, Size-Dependent Thermal Boundary Resistance and Thermal Conductivity in Si/Ge Core-Shell Nanowires, IEEE Trans. Electron Devices, 65 (2018) 361-366. https://doi.org/10.1109/Ted.2017.2771824

[12] E. Lee, T. Zhang, T. Yoo, Z. Guo, T. Luo, Nanostructures Significantly Enhance Thermal Transport across Solid Interfaces, ACS Appl Mater Interfaces, 8 (2016) 35505-35512. https://doi.org/10.1021/acsami.6b12947

[13] L. Yates, J. Anderson, X. Gu, C. Lee, T. Bai, M. Mecklenburg, T. Aoki, M.S.

Journal Pre-proofs

Goorsky, M. Kuball, E.L. Piner, S. Graham, Low Thermal Boundary Resistance Interfaces for GaN-on-Diamond Devices, ACS Appl Mater Interfaces, 10 (2018) 24302-24309. https://doi.org/10.1021/acsami.8b07014

[14] Y. Zhou, J. Anaya, J. Pomeroy, H. Sun, X. Gu, A. Xie, E. Beam, M. Becker, T.A. Grotjohn, C. Lee, M. Kuball, Barrier-Layer Optimization for Enhanced GaN-on-Diamond Device Cooling, ACS Appl Mater Interfaces, 9 (2017) 34416-34422. https://doi.org/10.1021/acsami.7b08961

[15] E.T. Swartz, R.O. Pohl, Thermal-Boundary Resistance, Rev. Mod. Phys., 61 (1989) 605-668. https://doi.org/10.1103/RevModPhys.61.605

[16] S. Mandal, C. Yuan, F. Massabuau, J.W. Pomeroy, J. Cuenca, H. Bland, E. Thomas, D. Wallis, T. Batten, D. Morgan, R. Oliver, M. Kuball, O.A. Williams, Thick, Adherent Diamond Films on AlN with Low Thermal Barrier Resistance, ACS Appl Mater Interfaces, 11 (2019) 40826-40834. https://doi.org/10.1021/acsami.9b13869

[17] Z. Cheng, T. Bai, J. Shi, T. Feng, Y. Wang, M. Mecklenburg, C. Li, K.D. Hobart, T.I. Feygelson, M.J. Tadjer, B.B. Pate, B.M. Foley, L. Yates, S.T. Pantelides, B.A. Cola, M. Goorsky, S. Graham, Tunable Thermal Energy Transport across Diamond Membranes and Diamond–Si Interfaces by Nanoscale Graphoepitaxy, ACS Appl. Mater. Interfaces, 11 (2019) 18517-18527. https://doi.org/10.1021/acsami.9b02234

[18] E. Lee, E. Menumerov, R.A. Hughes, S. Neretina, T. Luo, Low-Cost Nanostructures from Nanoparticle-Assisted Large-Scale Lithography Significantly Enhance Thermal Energy Transport across Solid Interfaces, ACS Appl. Mater. Interfaces, 10 (2018) 34690-34698. https://doi.org/10.1021/acsami.8b08180

[19] Y.-C. Hua, B.-Y. Cao, Study of phononic thermal transport across nanostructured interfaces using phonon Monte Carlo method, Int. J. Heat Mass Transfer, 154 (2020). https://doi.org/10.1016/j.ijheatmasstransfer.2020.119762

[20] X.G. Liang, L. Sun, Interface structure influence on thermal resistance across double-layered nanofilms, Microscale Thermophys. Eng., 9 (2005) 295-304. https://doi.org/10.1080/10893950500196469

[21] L. Tao, S. Theruvakkattil Sreenivasan, R. Shahsavari, Interlaced, Nanostructured

Journal Pre-proofs

Interface with Graphene Buffer Layer Reduces Thermal Boundary Resistance in Nano/Microelectronic Systems, ACS Appl Mater Interfaces, 9 (2017) 989-998. https://doi.org/10.1021/acsami.6b09482

[22] M. Hu, X.L. Zhang, D. Poulikakos, C.P. Grigoropoulos, Large "near junction" thermal resistance reduction in electronics by interface nanoengineering, Int. J. Heat Mass Transfer, 54 (2011) 5183-5191. https://doi.org/10.1016/j.ijheatmasstransfer.2011.08.027

[23] A.M. Joseph, B.Y. Cao, An electron-phonon Monte Carlo study on thermal transport in GaN, Int. J. Therm. Sci., 181 (2022). https://doi.org/10.1016/j.ijthermalsci.2022.107742

[24] M. Khalkhali, F. Khoeini, Impact of torsion and disorder on the thermal conductivity of Si nanowires: A nonequilibrium molecular dynamics study, J. Phys. Chem. Solids, 112 (2018) 216-221. https://doi.org/10.1016/j.jpcs.2017.09.032

[25] F. Bernardini, V. Fiorentini, D. Vanderbilt, Spontaneous polarization and piezoelectric constants of III-V nitrides, Physical Review B, 56 (1997) R10024. https://doi.org/10.1103/PhysRevB.56.R10024

[26] S. Plimpton, Fast Parallel Algorithms for Short-Range Molecular-Dynamics, J. Comput. Phys., 117 (1995) 1-19. https://doi.org/10.1006/jcph.1995.1039

[27] M. Tungare, Y.F. Shi, N. Tripathi, P. Suvarna, F. Shahedipour-Sandvik, A Tersoff-based interatomic potential for wurtzite AlN, Physica Status Solidi a-Applications and Materials Science, 208 (2011) 1569-1572. https://doi.org/10.1002/pssa.201001086

[28] J. Nord, K. Albe, P. Erhart, K. Nordlund, Modelling of compound semiconductors: analytical bond-order potential for gallium, nitrogen and gallium nitride, Journal of Physics-Condensed Matter, 15 (2003) 5649-5662. https://doi.org/10.1088/0953-8984/15/32/324

[29] P. Erhart, K. Albe, Analytical potential for atomistic simulations of silicon, carbon, and silicon carbide, Physical Review B, 71 (2005). https://doi.org/10.1103/PhysRevB.71.035211

[30] Q. Wang, N. Gui, X. Zhang, X. Yang, J. Tu, S. Jiang, Diffusion and thermo-

Journal Pre-proofs

driven migration of silver, palladium, and ruthenium nanoparticles in cubic SiC matrix using molecular dynamics, Int. J. Heat Mass Transfer, 197 (2022) 123359. https://doi.org/10.1016/j.ijheatmasstransfer.2022.123359

[31] P. Jund, R. Jullien, Molecular-dynamics calculation of the thermal conductivity of vitreous silica, Physical Review B, 59 (1999) 13707-13711. https://doi.org/10.1103/PhysRevB.59.13707

[32] J.P. Freedman, J.H. Leach, E.A. Preble, Z. Sitar, R.F. Davis, J.A. Malen, Universal phonon mean free path spectra in crystalline semiconductors at high temperature, Sci Rep, 3 (2013) 2963. https://doi.org/10.1038/srep02963

[33] T.-R. Hsu, MEMS and microsystems: design, manufacture, and nanoscale engineering, John Wiley & Sons, 2008.

[34] P.K. Schelling, S.R. Phillpot, P. Keblinski, Comparison of atomic-level simulation methods for computing thermal conductivity, Physical Review B, 65 (2002). https://doi.org/10.1103/PhysRevB.65.144306

[35] X.P. Zhao, X. Qian, X.B. Li, R.G. Yang, Thermal conductance of nanostructured interfaces from Monte Carlo simulations with ab initio-based phonon properties, J. Appl. Phys., 129 (2021). https://doi.org/10.1063/5.0050175

[36] M.P. Allen, D.J. Tildesley, Computer simulation of liquids, Oxford university press, 2017.

[37] M. Hu, P. Keblinski, P.K. Schelling, Kapitza conductance of silicon-amorphous polyethylene interfaces by molecular dynamics simulations, Physical Review B, 79 (2009). https://doi.org/10.1103/PhysRevB.79.104305

[38] M. Hu, P. Keblinski, J.S. Wang, N. Raravikar, Interfacial thermal conductance between silicon and a vertical carbon nanotube, J. Appl. Phys., 104 (2008) 083503. https://doi.org/10.1063/1.3000441

Journal Pre-proofs

Highlights

1. Thermal transport simulation of AlN/diamond nanostructured heterostructure was performed by molecular dynamics.

2. The AlN/diamond nanostructured interface could achieve a 28.18% reduction in thermal boundary resistance compared to the planar interface.
3. The effect of the nanopillar height was analyzed and optimized to achieve a minimum thermal boundary resistance of the AlN/diamond interface.
4. Relationship between the vibrational density of state at the AlN/diamond interface and thermal transport performance was clarified.

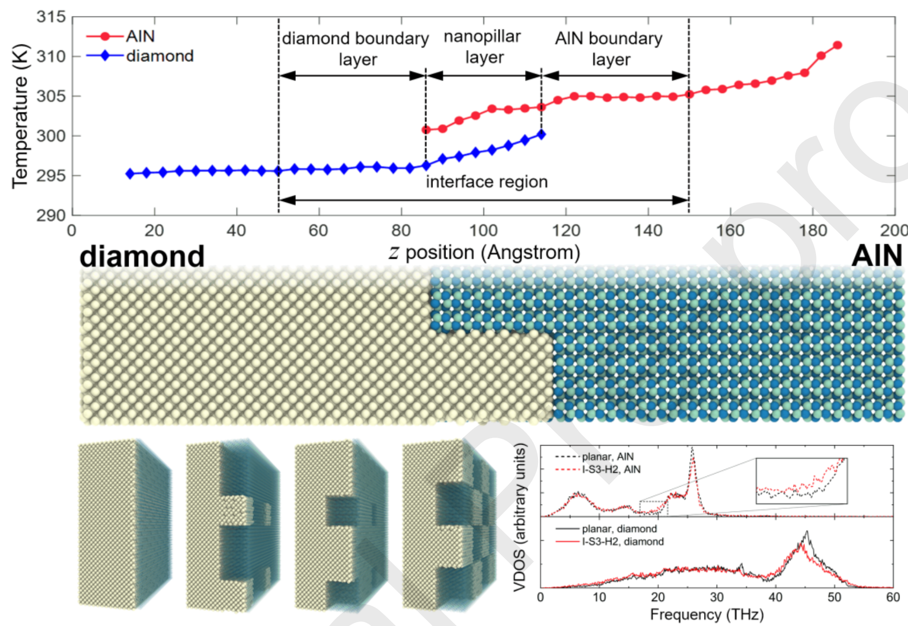

Zijun Qi and Wei Shen contributed equally to this work;

Zijun Qi: Conceptualization, Investigation, Methodology, Writing - Original Draft;

Wei Shen: Investigation, Methodology, Writing - Original Draft;

Rui Li: Review & Editing, Methodology;

Xiang Sun: Methodology, Formal analysis;

Lijie Li: Review & Editing;

Qijun Wang: Formal analysis;

Kang Liang: Review & Editing, Methodology, Software;

Gai Wu: Review & Editing, Conceptualization, Supervision, Resources, Funding Acquisition.

Journal Pre-proofs

Declaration of Competing Interest

The authors declare that they have no known competing financial interests or personal relationships that could have appeared to influence the work reported in this paper.

Journal Pre-proofs